Acta Astronautica 146 (2018) 409–417

Contents lists available at ScienceDirect

Acta Astronautica

journal homepage: www.elsevier.com/locate/actaastro

Mission analysis for the Martian Moons Explorer (MMX) mission☆

Stefano Campagnola[a,*], Chit Hong Yam[b], Yuichi Tsuda[c], Naoko Ogawa[c], Yasuhiro Kawakatsu[c]

[a] Jet Propulsion Laboratory, NASA, 4800 Oak Grove Dr, Pasadena, CA, 91109, USA
[b] ispace, inc., 3-1-6, Azabudai, Minato, Tokyo, 106-0041, Japan
[c] Institute of Space and Astronautical Science, JAXA, 3-1-1 Yoshinodai, Sagamihara, Kanagawa, 229-8510, Japan

ARTICLE INFO

Keywords:
MMX
Mars Phobos Deimos
Sample return mission
JAXA

ABSTRACT

Mars Moon eXplorer (MMX) is JAXA's next candidate flagship mission to be launched in the early 2020s. MMX will explore the Martian moons and return a sample from Phobos. This paper presents the mission analysis work, focusing on the transfer legs and comparing several architectures, such as hybrid options with chemical and electric propulsion modules. The selected baseline is a chemical-propulsion Phobos sample return, which is discussed in detail with the launch- and return-window analysis. The trajectories are optimized with the jTOP software, using planetary ephemerides for Mars and the Earth; Earth re-entry constraints are modeled with simple analytical equations. Finally, we introduce an analytical approximation of the three-burn capture strategy used in the Mars system. The approximation can be used together with a Lambert solver to quickly determine the transfer Δv costs.

1. Introduction

The Martian moons Phobos and Deimos hold the keys to understanding the origin and formation of the Solar System in general, and of Mars in particular. For this reason, in the last decade several space agencies have studied mission options dedicated to their exploration. In 2011, the Russian Space Agency launched the sample return Phobos-Grunt [1], but the spacecraft failed to escape the Earth system. More recently, several mission options were proposed by ESA and NASA (Phootprint [2], PANDORA [3], PADME [4], and MERLIN [5]), including flyby missions, orbiters, landers, and sample return missions.

Building on the experience of asteroid sample return spacecraft Hayabusa [6] and Hayabusa2 [7], JAXA is planning to launch the Mars Moon eXplorer (MMX) [8] in the early 2020s. MMX is a Martian moon explorer and a Phobos sample-return mission, and it is currently the main candidate for the next JAXA large-class mission, following Hayabusa 2 (currently flying) and the space observatory Hitomi/ASTRO-H (launched in 2016).

This paper presents the mission analysis work for MMX, in particular the transfers from the Earth to the moons, and from the moons back to the Earth. Several options are considered that differ in the propulsion system, the launch and return dates, and the moon or moons chosen for the sample collection. The current nominal scenario is also presented, a chemical-only Phobos sample return, with launch in 2022 and Earth re-entry in 2027. Finally, we present some useful analytical formulations to support the preliminary design, including a quick estimate of the three-maneuver strategy for orbit insertion (or escape) into Phobos orbit.

2. Martian Moon eXplorer (MMX)

2.1. Science objectives

Mars missions have traditionally addressed questions about the history of the surface environment and about climate change. But Mars system exploration can also shed light on how water was delivered to the rocky planets, since Mars was at a gateway position to witness the process of water transport by small bodies across the snow line, the distance from the Sun beyond which water ice can be stable. By exploring the Martian system and returning samples from Phobos,[1] MMX would investigate the origin of the Martian moons, and address fundamental questions of planetary system formation and of primordial material transport around the border between the inner- and the outer-part of the early Solar System.

Currently, the prevailing hypotheses on the origin of the Martian moons [9,10] are 1) the moons are captured primordial, type C or D

☆ This work was carried when all the authors were at the Institute of Space and Astronautical Science, JAXA.

* Corresponding author.
E-mail address: stefano.campagnola@jpl.nasa.gov (S. Campagnola).

[1] Currently, Phobos is the preferred target since it is more likely to have material ejected from Martian impact events. However, mission scenarios with sample acquisitions from Deimos are also under consideration.

https://doi.org/10.1016/j.actaastro.2018.03.024
Received 30 November 2017; Received in revised form 9 March 2018; Accepted 12 March 2018
Available online 15 March 2018
0094-5765/

asteroids, 2) the moons are remnants of Mars formation, or 3) the moons were formed by accretion of ejecta from a planetesimal impact on Mars. The sample analysis would solve the mystery of the origins of Deimos and Phobos, and characterize the transport of water (in case of 1), or the composition of Mars primordial material (in case of 2), or the composition of both Mars and of the impactor material (in case of 3). MMX would also address questions about the evolution of the surface of the moons (as compared to the surface of asteroids), and about the temporal and global distribution of atmospheric processes on Mars.

The spacecraft would be equipped with a sampler, capable of collecting 10 kg of material; several remote-sensing instrument such as a camera, a LIDAR, a near-IR spectrometer (for Mars atmospheric observations and for spectroscopy of the mineralogical signature),and a gamma-ray/neutron spectrometer (for elemental composition); and in-situ observation instruments for Phobos exploration such as an Ion mass spectrometer (for ice outgassing), and a dust counter.

2.2. Engineering objectives

MMX has also a number of engineering objectives aimed to improve JAXA's exploration capabilities for future space missions. For example, the roundtrip to Mars requires a large amount of energy (5 km/s of impulsive ΔV) that will be provided by one of the largest and most complicated chemical propulsion systems ever developed for a deep-space exploration spacecraft. Also, higher performance for the sample retrieval technology is required, compared to that used for Hayabusa and Hayabusa2. Science needs 10 g of samples (two orders of magnitude higher than Hayabusa2) from deeper than 2 cm, which requires a new corer and manipulator sampling technology, and to land and stay a few hours on the Martian moon.

2.3. Spacecraft overview

The current baseline scenario for MMX is a chemical propulsion mission, which is presented in detail in the next section. An artistic rendering of an example configuration [8] is shown in Fig. 1, where the spacecraft is composed of a return module (1350 kg), an exploration module (150 kg) and a propulsion module (1990 kg) for a total 3400 kg of wet mass at launch.

2.3.1. Planetary protection

Phobos and Deimos are in a gray zone concerning the level of planetary protections requirements [11], because of the recent hypotheses about their origin (they used to be in the same planetary protection category of near-Earth asteroids). MMX will need to minimize the risk of contamination of both the Mars system by the spacecraft, and of the Earth by the sample. In terms of trajectory design, an impact analysis has not been carried out yet, but we assume that the upper-stage trajectory will not be on a direct collision course with Mars, and a small trajectory correction maneuver will be performed by the spacecraft after launch to target the Mars approach. This offset targeting is the standard approach used to fulfill the planetary protection requirements for Mars when using direct escape launches [12]; a similar approach will be implemented for the return leg.

Fig. 1. Example configuration of the Mars Moon eXplorer (MMX).

Table 1
Phobos and Deimos orbital elements (ECLIPJ2000 centered in Mars).

Moon	a, *km*	e	incl.,^{o}	RAAN,^{o}	ω,^{o}
Phobos	9378.301	0.001482	25.7	82.3	274.5
Deimos	23459.16	0.000250	24.3	80.5	40.5

3. Mission architectures, baseline selection

A sample return mission to Phobos includes a round trip to the Mars system, proximity operations, landing and take-off. This paper presents multiple architectures for the round-trip transfer alone, which requires a large amount of propellant (about 4 km/s of impulsive Δv, more than in any other deep space mission from JAXA). Options for Deimos exploration are briefly discussed, but details about rendezvous operations for both moons, and landing and take-off operations at Phobos are not investigated; we simply assume at this stage that the correct phasing and approach geometry between MMX and Phobos can be attained with small trajectory correction maneuvers, without affecting the main results.

In this work we use SPICE ephemerides DE430 for the position of Mars and the Earth, and the SPICE kernels pck00010.tpc, gm_de431.tpc, naif0011.tls for the other planetary and time parameters. The orbital elements of Phobos and Deimos orbits on the Ecliptic are taken at an example epoch (Jun 21, 2024), and shown in Table 1.

3.1. Mission options

This section presents the trade-offs between trajectory options, which differ by launch date, propulsion system (chemical “CP”, or electric “EP”), and science phase duration.

Fig. 2 shows a selection of mission architectures, with their timelines and an estimate of the ratio between return mass and launch mass. In the table, case 1) represents a fast, CP-only transfer with a one-year stay at Mars, and Earth return in 2025. Case 5) is also a CP-only transfer, but with a 3-year stay at Mars and Earth return in 2027. Cases 4-d) and 4-e) implement EP and Mars gravity assists in the return leg to increase the spacecraft mass margin. (The case ID comes from the MMX project feasibility study documents).

The baseline scenario is selected after comparing the different options and trading mission risks, costs and scientific return. The first consideration is programmatic: if selected, MMX would follow Hayabusa2 (launched in 2014 [13]) and Hitomi/ASTRO H (launched in 2016) as JAXA's next large class mission.[2] A launch in the early 2020s is preferable as it fits well in JAXA's roadmap for planetary exploration. Also, a simple, quick transfer to Phobos minimizes the mission risks before the start of the science phase. For these reasons, fast, CP-only transfers are chosen for the Earth-Mars leg, with launch in 2022 or 2024.

For the return leg, hybrid EP/CP architectures become more attractive. The higher risks associated to EP can be tolerated, because most of the science is accomplished already during the science phase. Also, mass savings for the return module are beneficial for the Earth-Mars leg, since less propellant must be carried along. On the other hand,

[2] JAXA large class missions use the most powerful and expensive JAXA launchers (*H* type) and have budgets of USD ~300 M. BepiColombo's MMO is an international collaboration and falls into a different class.

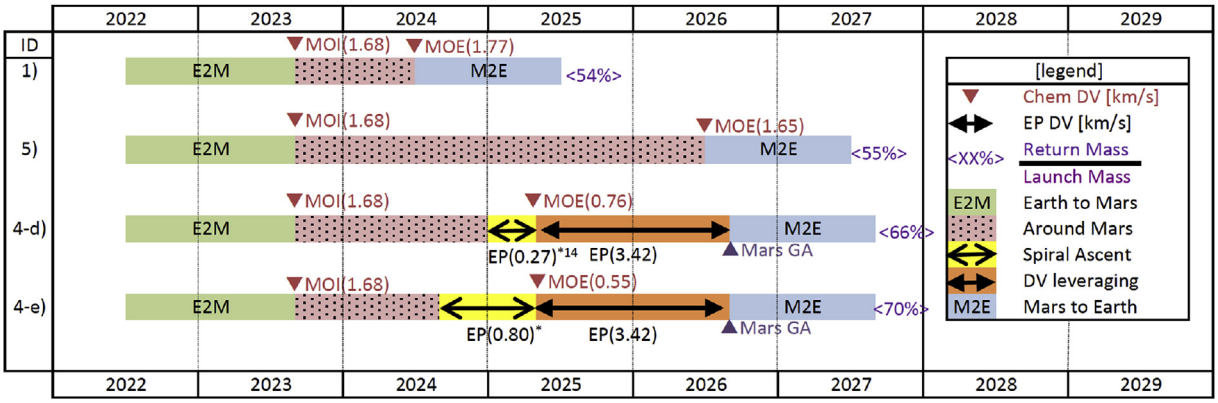

Fig. 2. MMX selected round-trip options.

EP/CP options increase not only the spacecraft and operation complexity and cost, but also the exposure of the sample to radiation. For these reasons, the CP propulsion options are preferred as long as they provide sufficient mass margin.

The duration of the science phase is also the subject of trade-offs. Scientists recommend at least a one-year stay at Mars and Phobos for science investigations, and ideally, up to 4 years. On the other hand, the science phase after the sample collection should be as short as possible, to reduce the radiation exposure and therefore the mass shielding.

The relative geometry between Earth, Mars, and the Sun is important to determine the science phase duration. Fig. 3 shows the distance between the Earth and Mars during the 2020s, which affects the telecommunication data rate. The figure also shows Sun occultations, where communication with the spacecraft is precluded because the Sun is within 5° from Mars, as seen from the Earth. The figure shows that the 2024–2025 time frame is optimal for telecommunication, while a science phase limited to 2023–2024 would suffer from both the Sun occultation and from a low data rate. A three-year stay between 2023 and 2025 is thus preferable.

The combination of science requirements, engineering constraints, and programmatic considerations result in case 5 of Fig. 2 to be accepted as the current baseline.

3.2. Nominal trajectory

In the baseline scenario, the spacecraft is launched into Earth escape with a velocity $v_\infty = 4.078$ km/s. The launch mass varies from 2500 kg (with current performances of H-IIA 204) to 3500 kg (with projected H-III performances), as long as the v_∞ declination is below 30° (the latitude of the Tanegashima launch center).

Fig. 4 shows the interplanetary transfer of the nominal scenario, while Table 2 shows the Δv costs for a 20-day launch window. In some cases, a Deep-Space Maneuver (DSM, Δv_1) is performed during the Earth-Mars leg. The Δv cost of 1.68 km/s in the mission architecture summary Fig. 2 is the maximum over the launch window.

Fig. 5 shows the close-up of the Phobos approach phase, with the Mars Orbit Insertion (MOI) maneuver, the Inclination-Change (and Apocenter-Raise) Maneuver (ICM), and the Phobos Orbit Insertion (POI) maneuver.

After a 3-year science phase, a reversed sequence of events is implemented to escape the Mars system and bring back the sample to the Woomera desert in 2027. The escape trajectory is shown in Fig. 6, while Table 3 shows the *return* window, where we account for possible delays of the Phobos Orbit Escape. The required total Δv in Fig. 2 is the maximum over the window.

4. Design of the outbound leg

For the design of the outbound leg, we first compute all the single-

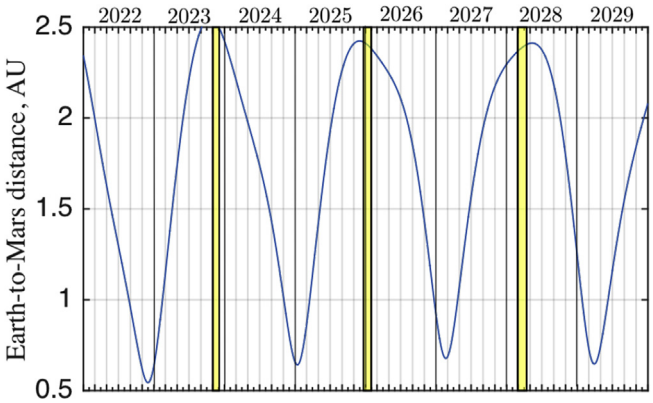

Fig. 3. Sun occultations and distance between the Earth and Mars during the 2020s.

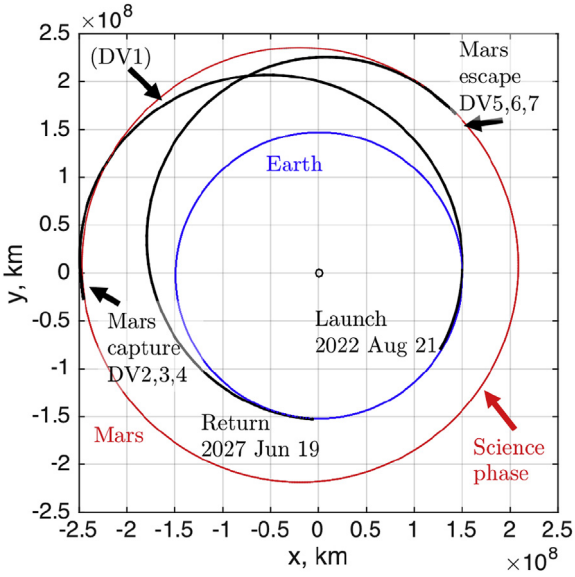

Fig. 4. Current MMX baseline (Ecliptic J2000).

revolution Lambert arcs with Earth departure and Mars arrival in the 2022–2029 time frame. Fig. 7 shows the transfers as segments connecting Earth departures (stars) with Mars arrivals (circles). For every launch date, only the transfer with the lower $v_{\infty Ea}$ is plotted, among those with $v_{\infty Ea} < 4.1$ km/s and $v_{\infty Ma} < 3$ km/s. The figure shows that launch opportunities open with the well-known 2-year cadence. The 2024 opportunity has an especially low $v_{\infty Ma}$.

At Mars arrival, impulsive maneuvers put the spacecraft in the same

Table 2
Launch window details.

Launch			Total Δv, km/s	DSM Δv_1		MOI Δv_2		ICM Δv_3		POI Δv_4	
Epoch, UTC	v_∞, km/s	δ, deg		Epoch, UTC	Δv, km/s	Epoch, UTC	Δv, km/s	Epoch, UTC	Δv, km/s	Epoch, UTC	Δv, km/s
2022 AUG 15	4.08	5.4	1.68	2022 DEC 19	0.15	2023 JUL 19	0.6	2023 JUL 22	0.12	2023 JUL 27	0.81
2022 AUG 16	4.08	5.1	1.66	2022 DEC 21	0.13	2023 JUL 20	0.61	2023 JUL 24	0.12	2023 JUL 29	0.81
2022 AUG 17	4.08	4.8	1.65	2022 DEC 23	0.1	2023 JUL 22	0.63	2023 JUL 26	0.12	2023 JUL 31	0.81
2022 AUG 18	4.08	4	1.64	2022 DEC 24	0.08	2023 JUL 23	0.64	2023 JUL 26	0.12	2023 JUL 31	0.81
2022 AUG 19	4.08	4.3	1.63	2022 DEC 27	0.05	2023 JUL 26	0.66	2023 JUL 30	0.12	2023 AUG 04	0.81
2022 AUG 20	4.08	4	1.62	2022 DEC 30	0.02	2023 JUL 28	0.67	2023 AUG 01	0.12	2023 AUG 06	0.81
2022 AUG 21	4.08	2.9	1.61	2022 DEC 29	0	2023 JUL 28	0.69	2023 AUG 01	0.12	2023 AUG 05	0.81
2022 AUG 22	4.06	2.2	1.62	2022 DEC 29	0	2023 JUL 28	0.69	2023 JUL 31	0.12	2023 AUG 05	0.81
2022 AUG 23	4.03	1.9	1.62	2022 DEC 30	0	2023 JUL 29	0.69	2023 AUG 02	0.12	2023 AUG 06	0.81
2022 AUG 24	4.01	1.7	1.63	2023 JAN 01	0	2023 JUL 30	0.7	2023 AUG 03	0.12	2023 AUG 08	0.81
2022 AUG 25	3.98	2	1.63	2023 JAN 03	0	2023 AUG 02	0.7	2023 AUG 05	0.12	2023 AUG 10	0.81
2022 AUG 26	3.96	1.8	1.64	2023 JAN 04	0	2023 AUG 03	0.71	2023 AUG 07	0.12	2023 AUG 11	0.81
2022 AUG 27	3.93	2	1.64	2023 JAN 05	0	2023 AUG 05	0.71	2023 AUG 09	0.12	2023 AUG 14	0.81
2022 AUG 28	3.92	1.7	1.65	2023 JAN 06	0	2023 AUG 06	0.72	2023 AUG 10	0.12	2023 AUG 15	0.81
2022 AUG 29	3.9	2.1	1.65	2023 JAN 08	0	2023 AUG 09	0.73	2023 AUG 12	0.12	2023 AUG 17	0.81
2022 AUG 30	3.88	2	1.66	2023 JAN 09	0	2023 AUG 10	0.73	2023 AUG 14	0.12	2023 AUG 18	0.81
2022 AUG 31	3.87	2	1.66	2023 JAN 11	0	2023 AUG 11	0.74	2023 AUG 15	0.12	2023 AUG 20	0.81
2022 SEP 01	3.86	1.9	1.67	2023 JAN 12	0	2023 AUG 13	0.74	2023 AUG 16	0.12	2023 AUG 21	0.81
2022 SEP 02	3.85	2.2	1.67	2023 JAN 13	0	2023 AUG 15	0.75	2023 AUG 18	0.11	2023 AUG 23	0.81
2022 SEP 03	3.84	2.3	1.68	2023 JAN 14	0	2023 AUG 16	0.76	2023 AUG 20	0.11	2023 AUG 25	0.81

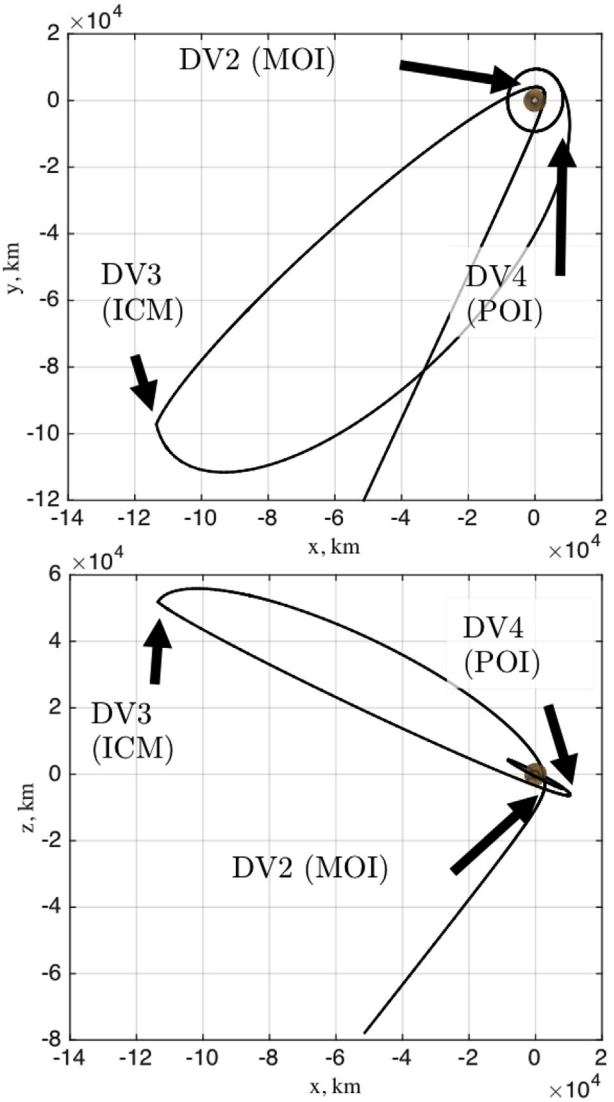

Fig. 5. Transfer to Phobos, details in the Mars system (Ecliptic J2000).

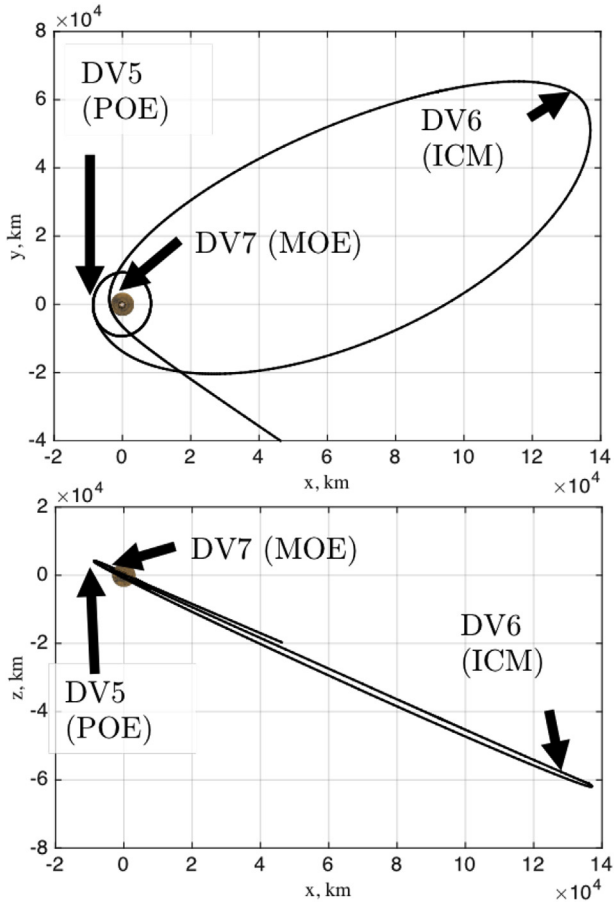

Fig. 6. Return trajectory, details in the Mars system (Ecliptic J2000).

orbit as Phobos. The sum of the impulsive maneuver Δvs are minimized with the jTOP software [14]. Constraints are added on the Earth escape conditions ($v_{\infty Ea}$ less than 4.078 km/s and with declination below 30°), and on the distance to Mars (minimum altitude 500 km, maximum distance after MOI 40 Mar radii). A first guess solution is built using 1) a Lambert arc with low $v_{\infty Ea}$ and low $v_{\infty Ma}$, 2) a hyperbolic approach trajectory in the Mars system, with low inclination to Phobos orbital

Table 3
Return window details.

Return			Total Δv, km/s	POE Δv_5		ICM Δv_6		MOE Δv_7	
Epoch, UTC	v_∞, km/s	δ, deg		Epoch, UTC	Δv, km/s	Epoch, UTC	Δv, km/s	Epoch, UTC	Δv, km/s
2027 JUN 10	3.02	−3.9	1.65	2026 JUL 16	0.81	2026 JUL 20	0.06	2026 JUL 24	0.78
2027 JUN 11	3.02	−3.8	1.65	2026 JUL 17	0.81	2026 JUL 21	0.06	2026 JUL 25	0.78
2027 JUN 12	3.02	−3.4	1.65	2026 JUL 18	0.81	2026 JUL 22	0.06	2026 JUL 26	0.77
2027 JUN 12	3.02	−3.1	1.64	2026 JUL 19	0.81	2026 JUL 23	0.06	2026 JUL 27	0.77
2027 JUN 12	3.02	−2.5	1.64	2026 JUL 20	0.81	2026 JUL 24	0.06	2026 JUL 28	0.77
2027 JUN 13	3.03	−2.5	1.64	2026 JUL 21	0.81	2026 JUL 25	0.06	2026 JUL 29	0.77
2027 JUN 15	3.04	−2.6	1.64	2026 JUL 22	0.81	2026 JUL 26	0.06	2026 JUL 30	0.77
2027 JUN 16	3.05	−2.6	1.64	2026 JUL 23	0.81	2026 JUL 27	0.06	2026 JUL 31	0.77
2027 JUN 16	3.06	−2.3	1.64	2026 JUL 24	0.81	2026 JUL 28	0.06	2026 AUG 01	0.77
2027 JUN 18	3.07	−2.3	1.64	2026 JUL 25	0.81	2026 JUL 29	0.06	2026 AUG 02	0.77
2027 JUN 19	3.09	−2.4	1.64	2026 JUL 26	0.81	2026 JUL 30	0.06	2026 AUG 03	0.77
2027 JUN 20	3.1	−2.2	1.64	2026 JUL 27	0.81	2026 JUL 31	0.06	2026 AUG 04	0.77
2027 JUN 21	3.12	−2.1	1.64	2026 JUL 28	0.81	2026 AUG 01	0.06	2026 AUG 05	0.77
2027 JUN 22	3.13	−2	1.64	2026 JUL 29	0.81	2026 AUG 02	0.06	2026 AUG 06	0.77
2027 JUN 23	3.16	−2	1.64	2026 JUL 30	0.81	2026 AUG 03	0.06	2026 AUG 07	0.77
2027 JUN 24	3.18	−2.1	1.64	2026 JUL 31	0.81	2026 AUG 04	0.06	2026 AUG 08	0.77
2027 JUN 25	3.2	−2	1.64	2026 AUG 01	0.81	2026 AUG 05	0.06	2026 AUG 09	0.77
2027 JUN 26	3.24	−2.2	1.64	2026 AUG 02	0.81	2026 AUG 06	0.06	2026 AUG 10	0.77
2027 JUN 27	3.27	−2.2	1.65	2026 AUG 03	0.81	2026 AUG 07	0.06	2026 AUG 11	0.77
2027 JUN 29	3.3	−2.2	1.65	2026 AUG 04	0.81	2026 AUG 08	0.06	2026 AUG 12	0.78
2027 JUN 30	3.35	−2.4	1.65	2026 AUG 05	0.81	2026 AUG 09	0.06	2026 AUG 13	0.78

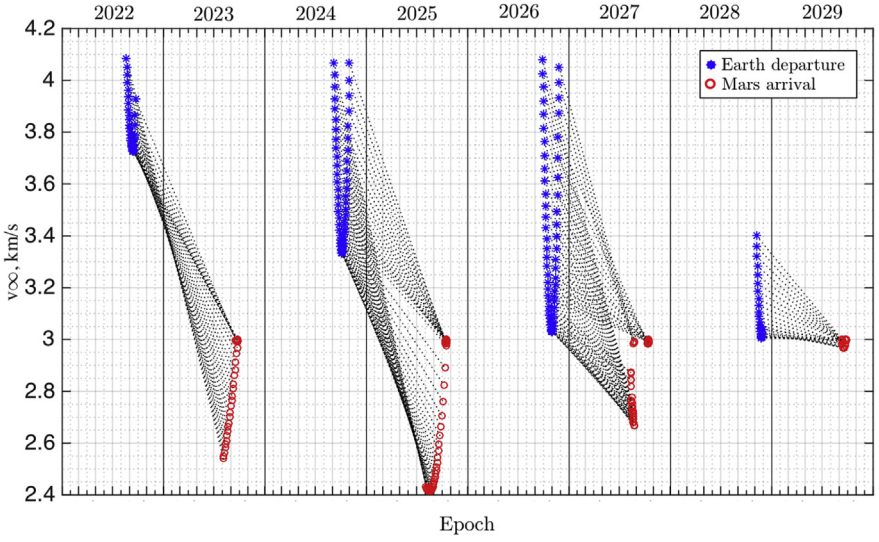

Fig. 7. Earth-to-Mars transfer opportunities.

plane, and closest approach at minimum altitude, 3) about half of a highly elliptical orbit, 4) and a low-Δv transfer to Phobos orbit.

The optimal solution for the 2022 opportunity is shown in Figs. 4 and 5. We discovered that, in the optimized solutions, a higher inclination of the approach hyperbola is traded for an eccentricity vector that is closer to Phobos orbital plane. Then, even after the MOI, the osculating apocenter remains close to Phobos orbital plane, and the following apocenter maneuver efficiently combines the plane change and pericenter raise maneuvers. We then derived an analytical approach to estimate the three-maneuver burn, for a given v_∞ magnitude and declination. The approach is explained in Appendix A, and will be used in future studies.

5. Phobos to earth

After about three years of in-situ and remote science in the Mars system, the spacecraft is ready to start its journey back to the Earth. For this part of the mission, we also consider electric propulsion options, which we did not consider in the initial leg.

5.1. Mars2Earth and chemical option

Fig. 8 shows the v_∞s of the Lambert arcs from Mars to Earth, with return opportunities every two years. For each departure date, the plot shows the minimum-$v_{\infty Ma}$ solutions, among those with $v_{\infty Ea} < 4$.

The Lambert arcs provide the direction and magnitude of the $v_{\infty Ma}$ needed to return to the Earth. In the chemical propulsion options, the required $v_{\infty Ma}$ is obtained with a three-impulse burn, which is the time reverse of the strategy used in the Earth-to-Phobos leg. Again the trajectories are optimized with jTOP, with constraints on the $v_{\infty Ea}$ to ensure a low-energy re-entry at the desired latitude (Woomera or Utah). The constraints are explained in Appendix B. The optimal solution for the 2026 return opportunity is shown in Figs. 4 and 6.

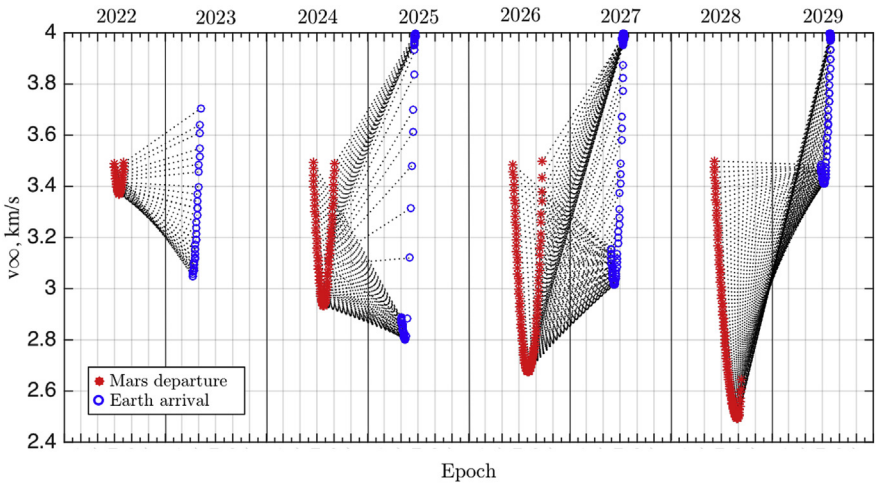

Fig. 8. Mars-to-Earth transfer opportunities.

5.2. Electric propulsion options

In the electric propulsion options, the required $v_{\infty Ma}$ is obtained with a low-thrust escape trajectory, followed by a low-thrust leveraging maneuver and a Mars gravity assist.[3] The low-thrust escape is presented first.

For this analysis, we assume an initial return module mass of 650 kg[4]; a CP engine with a specific impulse I_{sp} of 290s; and an EP module equipped with four μ10 Ion engines (I_{sp} = 2500s), three of which can be used at the same time for a total thrust of 30mN .

5.2.1. Hybrid EP-CP, parabolic escape

The simplest low-thrust escape trajectory starts from Phobos orbit and uses continuous tangential thrust plus a final impulsive maneuver to reach a parabolic escape. After escape, the spacecraft starts orbiting around the Sun close to Mars orbit. Because $v_{\infty Ma}$ is zero, there is no need to target a specific escape declination and the low-thrust spiral trajectory can lie on Phobos orbital plane (so no plane change maneuver is required).

The propellant mass and the time of flight depend on how much Δv is provided by the EP module, compared to the Δv provided by the CP maneuver. If little chemical propulsion is used, the total propellant mass is low (thanks to the lower I_{sp} of EP), but the transfer time is high. Fig. 9 shows the range of propellant mass, Δv, and the transfer time to reach Mars' sphere of influence. Each point in the curve represents a transfer, while the vertical dashed lines at 90 days and 240 days highlight the solutions used in cases 4-d and 4-e (see Fig. 2).

5.2.2. Alternative low-thrust escape approaches

The EP-CP strategy presented in the previous section is particularly simple and can quickly provide time-of-flight and propellant-mass figures. Other strategies were investigated and are reported here, although they did not improve (sufficiently) the results.

(1) In one approach, the EP arc is followed by a two-burn transfer, where the first burn is performed at apocenter and reduces the pericenter altitude, and the second burn is performed at pericenter to escape the Mars system. This strategy is similar to the impulsive, three-burn transfers used in the CP escape, except that a) the first chemical burn is replaced by the thrust arc, b) the transfer is planar, c) the escape is parabolic, not hyperbolic. A simple two-dimensional search showed that the optimal solutions have zero Δv in the first burn, similar to those computed in the previous section.

(2) In another approach, larger impulsive maneuvers provide hyperbolic escape conditions, reducing the EP mass requirements; however, more CP propulsion is needed and more propellant is also used to produce orbit plane changes.

(3) We also checked different thrust laws instead of the tangential one, and solved the optimal control problem by looping through all

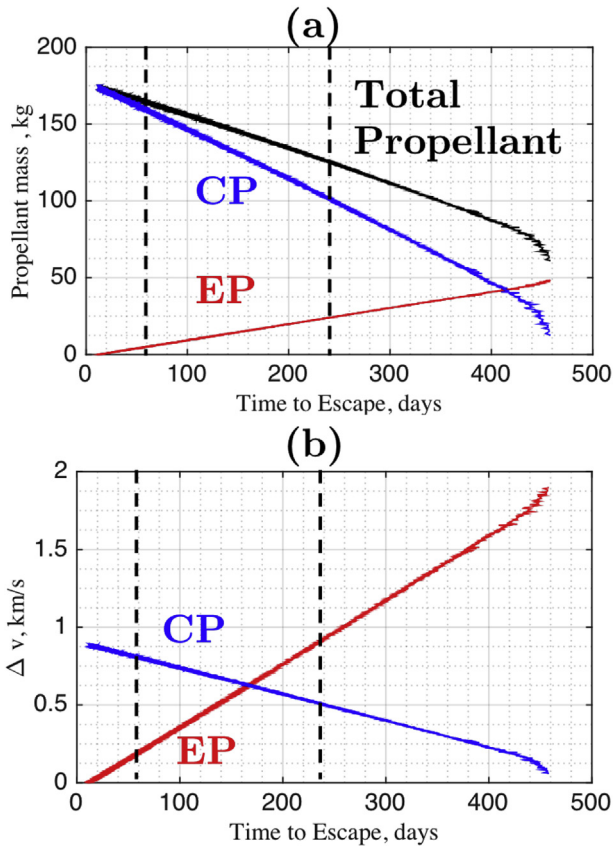

Fig. 9. Hybrid EP-CP escapes.

[3] A similar strategy with CP only was also briefly considered, but the project found the mass savings too small against the increased transfer time (operational costs) and risks. A leveraging maneuver on a 1:1 orbit is not as efficient in terms of ΔV as compared to a 2:1 for example, but it becomes more attractive when the longer transfer is exploited with long, high-I_{sp}, low-thrust arcs.

[4] The return module mass corresponds to a scenario with launch by H-IIA 204. If a H-III launcher is used instead, the return module mass would double but also the number of thrusters would double, and the results presented here would still hold in first approximation.

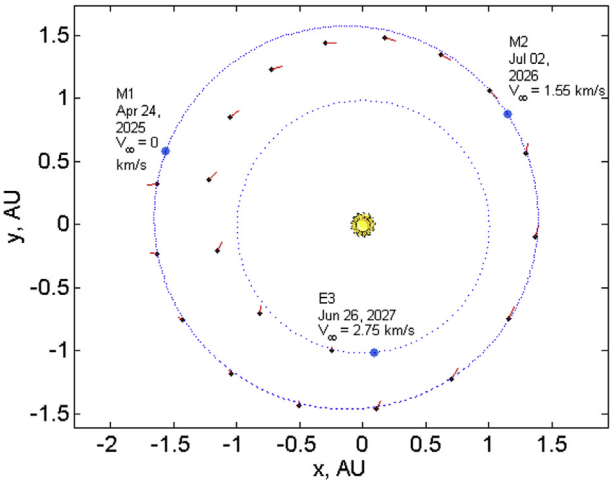

Fig. 10. Trajectory plot of a low-thrust Mars-Mars-Earth transfer trajectory using V_∞ leveraging via electric propulsion.

possible initial costates - but very small mass improvements are found, at the expense of longer computational times.

(4) Finally, we considered a strategy where an impulsive maneuver is applied first, and then the low-thrust arc is executed until reaching the sphere of influence. This strategy provides some significant savings only for very long solutions (>1 year).

(5) One approach we did not check is the low-energy escape that exploits Sun perturbation [15]. We don't expect such solution to significantly improve the propellant mass requirements for the short transfer times considered here (up to 8 months for escape).

5.2.3. Leveraging EP

With the EP scenario, the spacecraft is not able to go directly from Mars back to Earth since its escape C3 is not high enough. Instead, we use the technique of v_∞ leveraging via electric propulsion through a Mars-Mars transfer. Fig. 10 shows an example leveraging EP trajectory. The spacecraft spends about one year and three months to increase its $v_{\infty Ma}$ from zero to 1.5 km/s, before it performs a gravity assist at Mars to transfer back to the Earth a year later.

6. Deimos

Although Phobos is the main target of MMX, some options for the exploration of Deimos are also considered. Multiple Deimos flybys can be introduced at minimal cost during the capture or escape phase, but a higher scientific return is obtained with a Deimos-orbiting phase.

In general, it costs less to capture a spacecraft around Deimos than around Phobos, because Deimos is further outside in the gravitational well of Mars. A three-burn capture strategy as the one used in the nominal solutions costs about 300 m/s less, when the target moon is Deimos. However, a Hohmann transfer between the two moon requires 750 m/s. Overall, a mission that includes a Phobos sample return and a Deimos orbiter requires about 450 m/s more of total Δv.

7. Conclusion

This paper presented the mission analysis for the Mars Moon eXplorer mission, with focus on the transfer legs and on trade-offs between different architectures. We select as baseline the chemical-propulsion Phobos-sample-return option with launch in 2022 and Earth re-entry in 2027. The baseline is presented in detail with the launch and return window analysis. Finally, the paper also describes the trajectory design and optimization process, which is supported by some original analytical formulation.

Acknowledgment

Stefano Campagnola acknowledges the support of the JAXA International Top Young Fellowship program and of the KAKENHI-B grant #16K18311. Chit Hong Yam acknowledges the support of the Japan Society for the Promotion of Science (JSPS).

Appendix A. Three-burn strategy

For all the trajectories presented in this paper, the optimal timing, magnitude and direction of the burns at Mars arrival are found to be well approximated by a simple, three-burn strategy, where the periapsis of the incoming hyperbola lies on the $x-y$ plane defined by the target circular orbit. The strategy is composed of three burns, and efficiently combines the inclination change maneuver and periapsis raise maneuver at the first apocenter.

1. $\Delta V1$ is performed at the first periapsis, which is aligned with the node of the hyperbolic orbit; $\Delta V1$ is opposite to the velocity at periapsis, and injects the spacecraft into an elliptical orbit with a chosen apocenter radius (e.g. $40R_M$).
2. $\Delta V2$ is performed at the next apocenter, which also lies on the $x-y$ plane, and injects the spacecraft into a planar orbit with pericenter at the target circular orbit (e.g. orbital radius of Phobos).
3. The final $\Delta V3$ is performed at the second and final periapsis to circularize the elliptical transfer orbit.

The threeΔVs are quickly computed if the approach periapsis state vector is known. In the rest of the appendix, we show how to derive the orbital elements of the hyperbola (and therefore the periapsis state vector), given the incoming V_∞ vector and the periapsis distance.

We already know that the argument of the ascending node ω is either 0^o or 180^o, because the periapsis lies on the $x-y$ plane. We use the V_∞ magnitude in the vis-viva equation to compute the semi-major axis, and we use the periapsis distance to compute the eccentricity. To compute the inclination i and right ascension of the ascending node Ω, we use the definition of approach asymptote $\hat{\mathbf{V}}_\infty = V_\infty/\mathbf{V}_\infty$

$$\hat{\mathbf{V}}_\infty = (\cos\Omega\cos\theta - \sin\Omega\cos i\sin\theta)\hat{x} + (\sin\Omega\cos\theta + \cos\Omega\cos i\sin\theta)\hat{y} + (\sin i\sin\theta)\hat{z} \quad (1)$$

where $\theta = \omega + f_\infty$, and the incoming true anomaly f_∞ is given by

$$f_\infty = -\arccos(-1/e) \quad (2)$$

The three equations of Eq. (1) can then be finally solved for cosΩ, sinΩ, and i. Note that the third equation is the well-known relation between orbit inclination and V_∞ declination:

$$\sin\delta = \mp\sin i\sin(\omega + f_\infty) \quad (3)$$

where the $\mp$ sign denotes the incoming (−) and outgoing (+) cases.

Appendix B. Earth re-entry model

Table 4
Parameters for the Earth re-entry constraints.

v_{MAX}	γ^*	r^*	λ_W	λ_U
11.7 km/s	12.5°	6578.1366 km	− 30°	40°

The Earth return conditions are constrained such that an EDL sequence can be later designed for a Hayabusa-type capsule and landing sites in the Australian desert at Woomera or in the American desert in Utah. We used the parameters in Table 4 and implemented the simplifying assumptions:

(1) Maximum heating and heating rate constraints are satisfied if the speed and flight path angle at entry ($r_E = r*$) are

$$v_E \leq v_{MAX} \tag{4}$$

$$\gamma_E = \gamma^* \tag{5}$$

(2) The landing site is computed with a ballistic (i.e. with no drag) flight from the atmospheric entry time t_E to landing time t_L
(3) For this feasibility study, it is assumed that the landing longitude can be easily targeted in real operations by changing the landing hour with a small deep-space maneuver. The landing latitude, however, has to match that of one of the selected landing sites

$$\lambda_L \in \{\lambda_W, \lambda_U\} \tag{6}$$

In the rest of the appendix, equations (4)–(6) are transformed into two constraint equations for the v_∞ magnitude and declination δ.
We first derive the orbital elements of the entry hyperbola for a given v_∞^2 and γ_E. The semi-major axis is

$$a = -\frac{\mu_{Ea}}{v_\infty^2}$$

The momentum and eccentricity are

$$h = r^* v_E \cos\gamma_E$$

$$p = h^2/\mu_{Ea}$$

$$e = \sqrt{1 - \frac{p}{a}}$$

where the entry speed is

$$v_E = \sqrt{v_\infty^2 + \frac{2\mu_{Ea}}{r^*}}$$

The next equations provide the angle η between the incoming asymptote and the pericenter, the true anomaly at the landing site, and the angle θ between the landing site and the incoming asymptote (see Fig. 11)

$$\eta = \arccos(1/e)$$

$$f_L = -\arccos\left(\left(\frac{p}{r_L} - 1\right)/e\right)$$

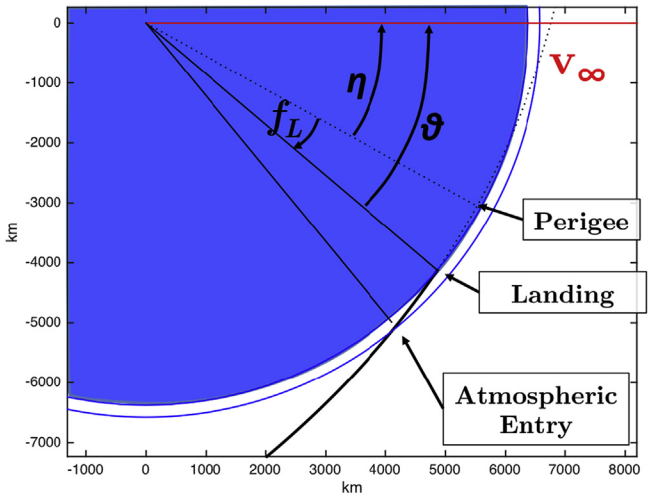

Fig. 11. Example reentry hyperbola.

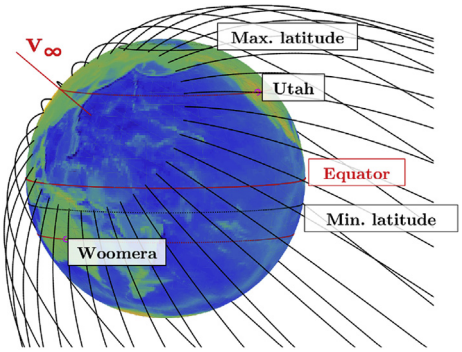

Fig. 12. Family of reentry hyperbolas.

$$\theta = \eta - f_L$$

Now we need to compute all the possible landing latitudes. Fig. 12 shows a family of hyperbolas, all with the same fixed v_∞. The landing locations lie on a circle with angular radius θ from the intersection of the v_∞ direction and the Earth surface. The figure also shows the circles of latitudes of Woomera and Utah, and the circles of minimum and maximum landing latitudes:

$$\lambda_{min} = \delta - \theta, \quad \lambda_{max} = \delta + \theta \tag{7}$$

Equation (7) is re-arranged to provide the second constraint equation

$$\lambda_{U,W} - \theta \leq \delta \leq \lambda_{U,W} + \theta \tag{8}$$

where only the latitude of the chosen landing site is used.

References

[1] M. Marov, V. Avduevsky, E. Akim, T. Eneeva, R. Kremnevc, S. Kulikovc, K. Pichkhadze, G. Popovd, G. Rogovskyc, Phobos-Grunt: Russian sample return mission, Adv. Space Res. 33 (12) (2004) 2276–2280, http://dx.doi.org/10.1016/S0273-1177(03)00515-5.

[2] D. Koschny, H. Svedhem, D. Rebuffat, Phootprint-A Phobos sample return mission study, 40th COSPAR Scientific Assembly, B0.4-9-14. URL http://adsabs.harvard.edu/abs/2014cosp…40E1592K.

[3] C. Raymond, T. Prettyman, S. Diniega, PANDORA-unlocking the mysteries of the moons of Mars, 46th Lunar and Planetary Conference, 2015.

[4] P. Lee, M. Benna, D. Britt, PADME (Phobos and Deimos and Mars environment): a proposed NASA discovery mission to investigate the two moons of Mars, 46th Lunar and Planetary Conference, 2015.

[5] S. Murchie, The mars-moons exploration, reconnaissance and landed investigation, 46th Lunar and Planetary Conference, 2015.

[6] J. Kawaguchi, A. Fujiwara, T. Uesugi, Hayabusa- its technology and science accomplishment summary and Hayabusa-2, Acta Astronaut. 62 (10–11) (2008) 639–647, http://dx.doi.org/10.1016/j.actaastro.2008.01.028.

[7] Y. Tsuda, M. Yoshikawa, M. Abe, System design of the Hayabusa 2 asteroid sample return mission to 1999 ju3, Acta Astronaut. 91 (2013) 356–362 http://www.sciencedirect.com/science/article/pii/S009457651300218X.

[8] Y. Kawakatsu, Martian Moons eXplorer (MMX) mission overview and current status, in: V.I. Misasa (Ed.), Frontiers in Earth and Planetary Materials Research: Origin, Evolution and Dynamics, 2016.

[9] S. Murchie, D. Britt, C. Pieters, The value of Phobos sample return, Planetary and Space Science 102 (1 November 2014) 176–182 http://www.sciencedirect.com/science/article/pii/S0032063314001123.

[10] J. Hopkins, W. Pratt, Comparison of Deimos and Phobos as destinations for human exploration, and identification of preferred landing sites, AIAA Space 2011 Conference & Exposition, 27-29 September 2011 Long Beach, CA, paper AIAA 2011-7140 https://doi.org/10.2514/6.2011-7140.

[11] P. Lee, K. Lorber, Phobos and Deimos: planetary protection knowledge gaps for human missions, Workshop on Planetary Protection Knowledge Gaps for Human Extraterrestrial Missions, 2015.

[12] J.M. Sánchez Pérez, Mission analysis guidelines MNSM-MAG-Issue 1-0, Tech. rep., European. Space Agency (2012) http://gpsm.spacescience.ro/ftp/vlad/Alpbach2014/files/usefull stuff/Peter Falkner/Mars/MNSM-MAG-Issue1–0.pdf.

[13] Y. Tsuda, S. Nakazawa, K. Kushiki, M. Yoshikawa, Flight status of robotic asteroid sample return mission Hayabusa2, Acta Astronautica. URL http://www.sciencedirect.com/science/article/pii/S0094576515302691.

[14] S. Campagnola, N. Ozaki, Y. Sugimoto, C.H. Yam, H. Chen, Y. Kawabata, S. Ogura, B. Sarli, Y. Kawakatsu, R. Funase, S. Nakasuka, Low-thrust trajectory design and operations of PROCYON, the first deep-space micro-spacecraft, 24th International Symposium on Space Flight Dynamics, Munich, Germany.

[15] F. Topputo, E. Belbruno, EarthMars transfers with ballistic capture, Celestial Mech. Dyn. Astron. 121 (4) (2015) 329–346, http://dx.doi.org/10.1007/s10569-015-9605-8.